The influence of edge sheared radial electric fields on edge-SOL coupling in the TJ-II stellarator

G. Grenfell[1,2], B.Ph. van Milligen[1], U. Losada[1], A. Cappa[1], T. Estrada[1],

M. Spolaore[2], C. Hidalgo[1] and the TJ-II Team

[1]*National Fusion Laboratory CIEMAT, 28040 Madrid, Spain*

[2]*Consorzio RFX, 35127, Padova, Italy*

The Scrape-Off Layer (SOL) profiles are determined by the competition between cross-field and parallel transport in magnetized plasmas [1]. While cross-field transport is typically turbulent and tends to enlarge the SOL width (λ_q), parallel transport acts as a fast dissipation mechanism along the field lines reducing the SOL profiles. From the present tokamak database, λ_q depends strongly on B_p [2], where B_p is the poloidal magnetic field at the outboard-midplane separatrix, resulting in a very tight operating margin for ITER [3]. However, recent simulations have shown that the SOL width in ITER might be larger than what would be expected in attached regimes [4]. The most plausible explanation is that the $E \times B$ shear in this device will not be strong enough to suppress and/or block the propagation of turbulent structures from the edge into the SOL.

The radial electric field (E_r) is a critical parameter for regulating cross-field transport, both in tokamaks and in stellarators. In the latter, the edge radial electric field depends on the interplay between neoclassical (NC) and turbulent mechanisms, where self-regulating phenomenons play a major role. During the electron ($E_r > 0$) to the ion root ($E_r < 0$) transition, E_r changes its sign in a continuous way [5]. This remarkable property makes stellarators ideal devices to investigate the connection between radial electric fields and edge-SOL coupling. In previous experiments, partial edge-SOL turbulence decoupling was achieved with the biasing electrode technique [6]. The aim of this work is to study the impact of a slowly vary radial electric field on turbulence propagation using the transfer entropy technique [10].

The current experiment was carried out in TJ-II (major radius $R_0 = 1.5$ m and minor radius $a < 0.22$ m) with magnetic field on axis $B_0 < 1.2$ T, and in the standard magnetic configuration, i.e. rotational transform $n/m = 8/5$ at $\rho \simeq 0.8$ (where ρ is the normalized flux coordinate). Deuterium plasmas were externally heated by two Electron Cyclotron Resonance Heating (ECRH) beamlines, delivering a total power of $P_{ECRH} \simeq 150$ kW. Two electrostatic probes toroidally displaced were used: probe B ($\phi = 195°$) inserted from the bottom and probe D ($\phi = 38°$) from the top.

Probe B is composed of 8 tips aligned radially and displaced ~ 2 mm from each other; all tips were set to measure floating potential (ϕ_f). Probe D is a 4x5 array of tips, with five rows radially displaced ~ 5 mm and having 4 tips each, spaced 3 mm poloidally. The measurement configuration was the following: [ϕ_+, ϕ_f, I_s, ϕ_f] in each row, where I_s is the ion saturation current and ϕ_+ is the positive potential for the triple probe configuration. In addition, TJ-II is equipped with two-channels of Doppler reflectometer [7], allowing to measure the plasma cross-field velocity with good spatial and temporal resolution.

Figure 1: *Plasma parameters during the electron-ion-electron root transition in the TJ-II: a) line averaged density and heating power, b) edge radial electric field (E_r) measure with Doppler reflectometry, and c) floating potential profile measured with the probe B.*

Fig. 1 shows: a) the central line-averaged density, b) the radial electric field at the plasma edge ($\rho \approx 0.8$) measured with Doppler reflectometry (by assuming that the intrinsic phase velocity is negligible compared to the $E \times B$ velocity [7]), and c) the time evolution of the floating potential radial profile measured with the probe B. In the first phase ($1100 \leq t \leq 1160$), the density increases from roughly 0.4 to $1.0 \cdot 10^{19}$ m^{-3} and the edge radial electric field changes sign in the electron to the ion root transition [5, 8]. The edge floating potential goes from positive to negative, followed by a flip of its gradient sign around the last closed flux surface (LCFS). During the ramp down ($1160 \leq t \leq 1250$), E_r changes sign again and so does the ϕ_f profile near the edge. Concomitantly, the ion saturation current decreases, while the electron temperature increases (both measured at $\rho \approx 0.9$, poster). The plasma in this stage returns to the electron root regime, but with a slightly lower density than before.

Zonal flows typically appear as global structure (exhibiting long-range correlation) during the root transitions due to a decrease of the neoclassical viscosity [5].
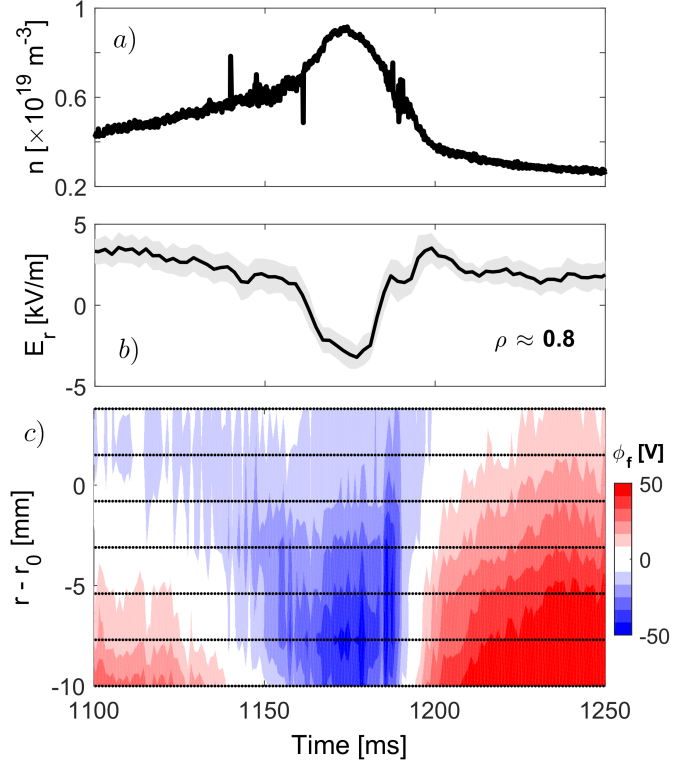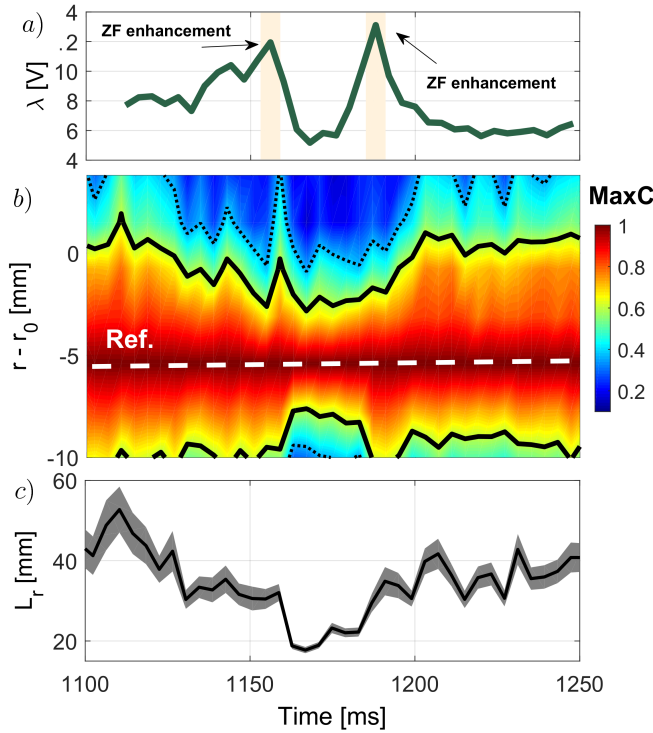
Figure 2: *At top: coefficient (λ) of the dominant global mode (related to zonal flows) calculated from ϕ_f signals from probes B and D by using the Singular Value Decomposition (SVD). At the center: profile of the maximum correlation (reference: $r - r_0 \approx -5$ mm) in time. The black continuous and dotted lines represent, respectively, the correlation at 0.6 and 1/e. At the bottom: effective radial correlation length computed from a double exponential fit starting from the reference position.*

Global structure related to zonal flows (ZF) has been identified unambiguously in TJ-II using biorthogonal decomposition considering multiple toroidally displaced signals [9]. Fig. 2 a) shows the time evolution of the ZF mode amplitude (λ), clearly peaking at the transitions. Fig. 2 b) shows the cross-correlation between floating potentials in probe B (bandwidth 2-600 kHz), where the chosen reference is in the edge. We considered the maximum correlation (at any time delay) in order to take into account turbulence propagation. One can see that the high correlation width is reduced in the ion root phase. This result can be better visualized by computing the correlation length. Fitting two exponential function starting from the reference, the effective radial correlation length (L_r) is the sum of the two exponential decay lengths. L_r (Fig. 2 c) varies from around 3.5 cm in the electron root to 2.0 cm in the ion root phase, suggesting turbulence is affected locally.

To measure radial turbulence propagation we used the Transfer Entropy (TE) technique [10]. The technique allows studying the causal relationship between two signals by measuring the amount of information exchanged between them in a defined direction and time delay. Given two-time series $x(t)$ and $y(t)$, the transfer entropy X to Y is:

$$T_{X \to Y} = \sum p(x_{n+1}, x_{n-k}, y_{n-k}) \log_2 \frac{p(x_{n+1} | x_{n-k}, y_{n-k})}{p(x_{n+1} | x_{n-k})} \tag{1}$$

Where $p(...)$ is the probability density function and $p(a|b) = p(a,b)/p(b)$ is the conditional

PDF. The probability density function is built by 'course graining', that is, by selecting a low bin number 'm' that gives statistically significant results.

Fig. 3 shows TE from the innermost floating potential ($r - r_0 \approx -10$ mm) in the probe B at different instants: (1) electron, (2) ion, and (3) electron root phase. The net information flow is predominately outward in the three cases. Initially (first frame), propagation flows at 1 km/s (deduced from the slope of the plume) up to the near SOL. In the ion root phase, propagation almost completely ceases, becoming restricted to a short range near the reference. In the back transition (third frame, electron root) the plume returns even stronger than before.
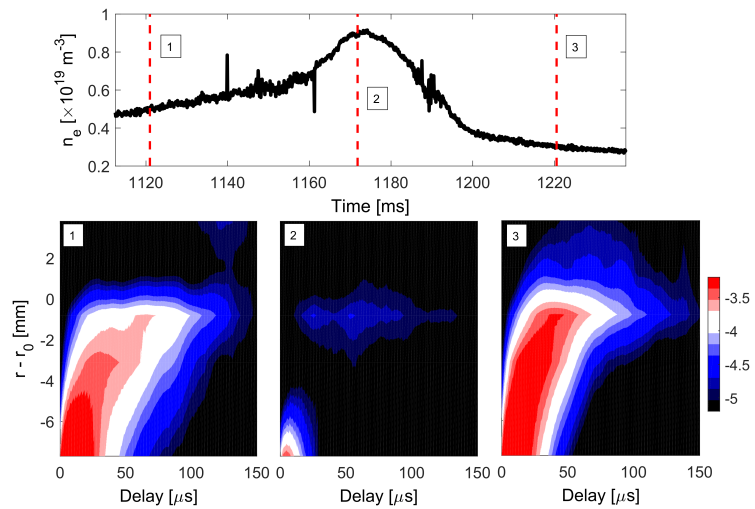

Figure 3: *Transfer entropy radial extension (reference: $r - r_0 \approx -10$ mm) at three time slices: 1 - electron root, 2 - ion root, and 3 - lower density electron root. At the top is shown the central line density with the indicated time slices (dashed vertical lines).*

We have shown that radial electric fields are not only able to modify turbulence locally, but also to affect its propagation. These results are particularly relevant for understanding the mechanisms that determine the SOL width, and to provide some hints on non-local processes and edge-SOL coupling.

References

[1] Stangeby, P.C. et al. Plasma Phys. Controlled Fusion 42.12B (2000)
[2] Eich, T. et al. Phys. Rev. Lett. 107, 215001 (2011)
[3] Kukushkin, A. et al. J. Nucl. Mat. 438, S203 (2013)
[4] Chang, C. et al. Nucl. Fusion 57, 116023 (2017)
[5] Velasco, J. L and Castejãşn, F. Plasma Phys. Control. Fusion 54, 015005 (2011)
[6] Grenfell, G. et al. Nucl. Fusion 59, 016018 (2018).
[7] Estrada, T. et al. Plasma Phys. Control. Fusion 51, 124015 (2009).
[8] Melnikov, A. et al. Nucl. Fusion 51, 083043 (2011)
[9] van Milligen, B. P. et al. Plasma Phys. Control. Fusion 57, 025005 (2014)
[10] van Milligen, B. P. et al. Nucl. Fusion 54, 023011 (2014)